BIOCHEMISTRY
including biophysical chemistry & molecular biology

Article

pubs.acs.org/biochemistry

Conformational and Dynamic Changes at the Interface Contribute to Ligand Binding by Ubiquitin

Monica Sundd*

National Institute of Immunology, Aruna Asaf Ali Marg, New Delhi 110 067, India

Supporting Information

ABSTRACT: Ubiquitin interacts with numerous domains and motifs in its lifetime that vary in structure but bind the same hydrophobic patch. To identify the structural features of ubiquitin that make it an exceptional protein−protein interaction partner, we have studied the interaction of ubiquitin with the signal transducing adaptor molecule-1 ubiquitin interacting motif (UIM) using nuclear magnetic resonance. Our studies bring to light the role of the inherent backbone flexibility of ubiquitin in its interactions with a large array of binding partners, revealed from the changes in C_α chemical shifts, backbone dynamics, and hydrogen bond lengths upon UIM binding. The crystal structures of ubiquitin complexes lend further support to our findings, underscoring the importance of the unique and flexible hydrogen bond network within ubiquitin and simultaneously providing insights into the nature of the slow motions. Taken together, our studies provide an in-depth view of the molecular changes associated with ligand recognition by ubiquitin.

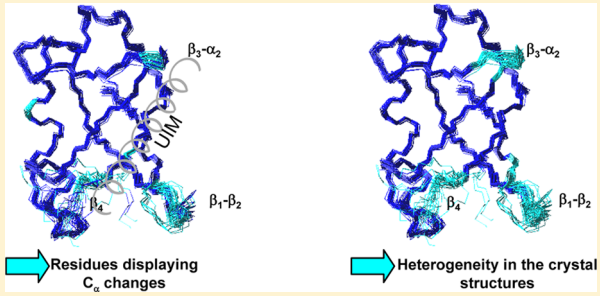

Ubiquitin is a remarkable protein, with innumerable noncovalent interactions playing a vital role in the regulation of a multitude of cellular processes. A diverse range of ubiquitin binding modular elements are known,[1−3] viz., α-helical (UIM) ubiquitin interacting motif, three-helix bundle (UBA), ubiquitin-associated domain, GAT, and CUE, with mixed $\alpha-\beta$ structure as in ubiquitin E2 variant domain (UEV), that bind ubiquitin with high specificity. Interestingly, these interactions can be grouped into three categories based on the binding site: (a) solvent-exposed hydrophobic patch surrounding Leu 8, Ile 44, and Val 70,[4] (b) the C-terminal tail encompassing Gly 76,[5] and (c) the Thr 55−Asn 60 region of ubiquitin.[6,7]

Comparison of the interaction surface of ubiquitin in its complexes suggests that majority of the interactions are mediated by the hydrophobic patch.[4] It is perplexing how a single ubiquitin molecule recognizes such a diverse range of binding partners. Given the structural diversity of its ligands and the variation in specificity, multiple structural determinants of ubiquitin recognition probably exist for each partner. Identification of the structural features of ubiquitin that play an indispensable role in its recognition is necessary to understand the regulation of ubiquitin-mediated pathways. A few recent studies have highlighted the importance of a rigid hydrophobic core, coupled to highly flexible side chains, in governing the recognition process of ubiquitin.[8,9] A recent review compared 24 molecules of ubiquitin obtained from 18 high-resolution X-ray structures and concluded that at least 39 residues in ubiquitin have flexible side chains while the rest form a conserved hydrophobic core.[10] Ubiquitin still remains a mystery with regard to its expanding number of interactions.

Ubiquitin−UIM interaction emerges as an ideal candidate for exploring the molecular mechanism of ubiquitin recognition, because of a large body of available structural data. Moreover, the interaction is highly important in endosomal sorting machinery (ESCRT), targeting ubiquitinated cargo to the late endosomes or lysosomes.[11] Biochemically, the interaction is akin to any other protein−protein interaction, primarily governed by hydrophobic and electrostatic forces.[12] The UIM attains a helix−loop−helix conformation, and the leucines of UIM interact with the three hydrophobic residues of ubiquitin, namely, Ile 44, Val 70, and Leu 8. The glutamates of UIM form electrostatic interactions with Arg 42, Arg 72, Lys 6, and Gly 47 of ubiquitin. Sequence comparison studies suggest that the UIM sequences can be narrowed down to the consensus sequence X-Ac-Ac-Ac-ϕ-X-X-Ala-X-X-X-Ser-X-X-Ac-X-X-X-X, where ϕ is a hydrophobic residue, Ac is an Asp or Glu, and X is a variable residue. The conserved residues in the aforementioned sequence of UIMs if mutated cause a marked reduction in binding affinity, and function, underscoring their importance in the interaction.[13] For example, mutation of a Ser residue eliminates ubiquitin binding completely in pull-down assays while mutation of Ala to an Asp weakens binding.[14]

A major bottleneck in characterizing protein−ligand interactions is their dynamic nature. It is difficult, if not impossible, to follow the changes upon ligand binding. Furthermore, it is challenging to experimentally trap and observe the weakly populated, ligand-bound conformations. At

Received: April 3, 2012
Revised: September 25, 2012
Published: October 4, 2012

dx.doi.org/10.1021/bi3004268 | *Biochemistry* 2012, 51, 8111−8124

this juncture, nuclear magnetic resonance (NMR) spectroscopy comes to the rescue. The sensitivity of NMR in the observation of the sparsely populated conformations and the tracking of their minutest changes is unmatched. Moreover, the technique works efficiently for extremely weak interactions, which are most commonly encountered in biological systems, and thus can be used to study motions anywhere in the millisecond to picosecond range.[15−18]

Using NMR, we have closely followed the changes in ubiquitin upon binding to a UIM of signal transducing adaptor molecule-1 (STAM1), a representative of the multiple ubiquitin binding domains present in the endosomal sorting complex transport (ESCRT) machinery. ESCRT proteins are important for endosomal sorting, and dysregulation of these proteins leads to cancer and even neurodegeneration.[19] A single ubiquitin modification is sufficient for the entry of the cargo protein into the multivesicular bodies.[20] We are trying to address the major question of the structural features of ubiquitin that impart it with the unique ability to bind a wide range of structures. Our studies shed light on the unusual backbone flexibility of ubiquitin, disclosed by the changes in backbone conformation, hydrogen bond lengths, and dynamics upon ligand binding. Besides, the unique hydrogen bond network that makes the surface of ubiquitin fluid-like is another important factor contributing to its remarkable ligand diversity.

EXPERIMENTAL PROCEDURES

Unlabeled and ^{15}N- and ^{13}C-labeled proteins were expressed in *Escherichia coli* and purified as described previously.[21]

Acquisition of NMR Data. NMR samples consisted of [U-^{1}H,^{15}N,^{13}C]protein, in 50 mM sodium phosphate buffer (pH 6.0), 0.5 mM sodium azide, 90% H_2O, and 10% D_2O. A protein concentration of 1−2 mM was used throughout this work. The STAM1 peptide with an "Ace-KEEEDLAKAIELS-LKEQRQQ-NH_2" sequence spanning residues 171−190 was chemically synthesized.

All NMR experiments were performed on a Bruker Avance III 700 MHz spectrometer equipped with a TCI cryoprobe installed at the National Institute of Immunology. NMR data were processed on a workstation running Red Hat Enterprise Linux 5.0, using NMRPipe/NMRDraw,[22] and analyzed using Sparky.[23] The data were multiplied by a phase-shifted sine bell apodization function in all dimensions.

^{1}H−^{15}N HSQC spectra were acquired using 1024 data points in the t_2 dimension and 512 data points in the t_1 dimension. CBCAcoNH, HNCACB, and HNcoCA spectra were acquired with 1024 (t_3) × 48 (t_1) × 24 (t_2) points. ^{13}C−^{15}N-filtered, ^{15}N-edited NOESY spectra were acquired with 1024 points in the t_3 dimension, 20 points in the t_2 dimension, and 40 points in the t_1 dimension. ^{1}H TOCSY spectra were acquired with 1024 points in the t_2 dimension and 512 points in the t_1 dimension. Data were linearly predicted in the forward direction for up to half the number of experimental points in the indirect dimensions. ^{15}N−^{13}C spectra were referenced indirectly using sodium 2,2-dimethyl-2-silapentane-5-sulfonate (DSS) as a standard.[24] For temperature studies, methanol was used as an external standard.[25]

For peptide titrations, ^{1}H- and ^{15}N-labeled ubiquitin was titrated with increasing concentrations of the unlabeled peptide in small aliquots (total volume of the added peptide of 50 μL). Nonlinear least-squares analysis of the chemical shift changes, $\Delta\delta/\Delta\delta_{max}$ (change in chemical shift/maximal change in chemical shift), as a function of ligand concentration was employed to determine estimates for K_d using the following equation:

$$\Delta\delta/\Delta\delta_{max} = f_b = \left[[P]_t + [L]_t + K_d \pm \sqrt{([P]_t + [L]_t + K_d)^2 - 4[P]_t[L]_t}\right] / (2[P]_t) \quad (1)$$

where $[P]_t$ represents the total concentration of the protein, $[L]_t$ represents the total concentration of the ligand, $\Delta\delta$ is the measured chemical shift change at each ligand concentration, and $\Delta\delta_{max}$ is the maximal change in chemical shift.[26]

Relaxation experiments (^{15}N T_1, ^{15}N T_2, and ^{15}N{^{1}H} NOE) were conducted on a Bruker Avance III 700 MHz NMR spectrometer at 278 K as described previously.[27] In the case of T_1 and T_2 measurements, 24 transients were acquired per experiment and a total of 256 (t_1) × 2048 (t_2) complex points were acquired. ^{15}N T_1 relaxation delays of 0.01, 0.02, 0.04, 0.08, 0.16, 0.32, 0.64, 0.96, and 1.28 s were used with the inversion recovery pulse sequence. ^{15}N T_2 Carr−Purcell−Meiboom−Gill (CPMG) relaxation rates were measured using a CPMG pulse sequence with relaxation delays of 0.01, 0.03, 0.05, 0.07, 0.09, 0.11, 0.13, 0.15, 0.17, 0.19, 0.21, 0.23, and 0.25 s. An interpulse delay of 0.9 ms was used between two ^{15}N 180° pulses in the CPMG sequence. NOE measurements were taken using a total of 32 transients per t_1 experiment with 2048 (t_2) × 128 (t_1) points.[27] A recycle delay of 1.5 s was used throughout this work. All three sets of experiments were acquired as duplicates.

^{15}N constant-time CPMG relaxation dispersion experiments were also conducted at 278 K on a 700 MHz NMR spectrometer equipped with a crypoprobe using pulse sequences as described previously.[28] Perdeuterated ^{15}N- and ^{13}C-labeled ubiquitin samples were used to observe the maximal contribution from the conformational exchange process. A τ_{CP} (constant-time delay) was set to 40 ms. A reference spectrum was acquired, without a constant-time CPMG element, along with 11 spectra with varying CPMG frequencies, viz., 25, 50, 100, 150, 200, 250, 300, 400, 600, 800, and 1000 Hz, in duplicate. Twenty-four scans per free induction decay (FID) were recorded with a relaxation delay of 2.5 s. The pseudo-three-dimensional data were processed using nmrPipe,[22] and peak intensities were measured using Sparky.[23]

Relaxation Data Analysis. The relaxation data were analyzed using Sparky.[23] Intensities of the amides were obtained by measuring heights of the peaks in the spectra, and T_1 and T_2 values were obtained by nonlinear regression of single-exponential decays. Uncertainty in peak height was determined from duplicate spectra acquired independently. Sparky2rate script (http://xbeams.chem.yale.edu/~loria/sparky2rateDr.PatrickJ.Loria, Yale University, New Haven, CT) based on CURVEFIT (A. G. Palmer III, Columbia University, New York, NY) was used to convert the relaxation time from the duplicate spectra into relaxation rates and to calculate the standard deviation. The ^{15}N{^{1}H} heteronuclear steady state NOE was calculated from the I_{sat}/I_{unsat} ratio, where I_{sat} and I_{unsat} are the peak intensities in the spectra collected with and without proton saturation, respectively.

^{15}N transverse relaxation data were analyzed using the extended model free approach using FAST-Modelfree.[29] A ^{15}N magnetogyric ratio of −2.71, a CSA of the ^{15}N atom of −160,

dx.doi.org/10.1021/bi3004268 | *Biochemistry* 2012, 51, 8111−8124

and an N−H bond distance of 1.02 Å were used. An axially symmetric model for rotational diffusion appeared to best fit the experimental data. An axially symmetric rotational diffusion tensor with a $D_{\parallel}/D_{\perp}$ ratio of 0.8 ± 0.01, a θ of −56.66, and a ϕ of −63.74 for free ubiquitin and a $D_{\parallel}/D_{\perp}$ ratio of 0.71 ± 0.01, a θ of −62.63, and a ϕ of −13.4 for ubiquitin bound to UIM were used. The following five models were used to describe the spin relaxation data: S^2 (model 1), S^2 and τ_e (model 2), S^2 and R_{ex} (model 3), S^2, τ_e, and R_{ex} (model 4), and S^2, τ_e, and S_f^2 (model 5). S^2 is the order parameter, with values between 0 and 1, used to fit the amplitude of internal motions on the picosecond to nanosecond time scale. S_f^2 is the order parameter for fast motions. τ_e is the effective correlation time for internal motions. R_{ex} represents chemical and/or conformational exchange for the microsecond to millisecond motions. A χ^2 test was used to confirm the goodness of fit.

In the case of ^{15}N transverse relaxation dispersion experiments, R_2^{eff} was extracted from a series of CPMG constant-time relaxation dispersion experiments using NESSY[30] according to the equation

$$R_2^{eff} = 1/T_{CPMG} \ln[I(0)/I(\nu_{CPMG})] \quad (2)$$

where T_{CPMG} is the constant CPMG time, $I(0)$ is the intensity of the peak in the reference spectrum, and $I(\nu_{CPMG})$ is the intensity of the peak at the CPMG frequency (ν_{CPMG}). Dispersion profiles of the residues were fit individually to different models that are distinguished from one another on the basis of the exchange processes using the automated fitting software NESSY:[30]

(a) Model 1 with no exchange, i.e., $R_2^{eff} = R_2^0$.

(b) Model 2 with two-state fast exchange:

$$R_2^{eff} = R_2^0 + \phi/k_{ex}\left[1 - \frac{4\nu_{CPMG}}{k_{ex}} \tanh(k_{ex}/4\nu_{CPMG})\right] \quad (3)$$

where $\phi = p_a p_b \delta\omega^2$.

(c) Model 3 with two-state slow exchange using the Richard−Carver equation[31] (eq 4)

$$R_2^{eff} = R_2^0 + k_{ex}/2 - n_{CPMG} \cosh^{-1}[D_+ \cosh(\eta_+) - D_- \cos(\eta_-)] \quad (4)$$

where

$$\nu_{CPMG} = (\tau_{cp} + p\omega_{180°})/2$$

$$D_{\pm} = \frac{1}{2}[\pm 1 + (\Psi + 2\delta\omega^2)/(\Psi^2 + \xi^2)^{1/2}]$$

$$\eta_{\pm} = [\pm\Psi + (\Psi^2 + \xi^2)^{1/2}]^{1/2}/(2\sqrt{2\nu_{CPMG}})$$

$$\Psi = k_{ex}^2 - \delta\omega^2$$

$$\xi = -2\delta\omega(p_a k_{ex} - p_b k_{ex})$$

where ν_{CPMG} is the field strength of the CPMG spin-echo pulses, τ_{cp} is the delay between two consecutive 180° ^{15}N refocusing pulses, $p\omega_{180°}$ is the pulse width, R_2^0 is the transverse relaxation rate constant in the absence of exchange, p_a and p_b are the equilibrium populations at the two sites, k_{ex} is the exchange rate constant, and $\delta\omega$ is the chemical shift difference between the two sites.

From this analysis, the following parameters were obtained: (a) the rates of interconversion (k_{ex}), (b) relative populations of exchanging species (p_b), (c) differences in chemical shifts between the two species ($\Delta\delta\omega_N$), and (d) χ_{res}^2 for individual fits. Global fitting of the residues was also conducted, and the sites experiencing conformational dynamics distinct from the global process were identified on the basis of the high $\chi_{group}^2/\chi_{res}^2$ ratio. This was an iterative fitting process, and the residues displaying a $\chi_{group}^2/\chi_{res}^2$ ratio of ≤2 were removed one by one from the cluster after each round of fitting, until all the fitted residues displayed a $\chi_{group}^2/\chi_{res}^2$ value of ≤2.

Trans Hydrogen Bond Scalar Couplings. Trans hydrogen bond scalar coupling ($^{h3}J_{NC'}$) experiments were conducted on an Avance III Bruker 700 MHz NMR spectrometer equipped with a triple-resonance TCI probe. A long-range HNCO experiment optimized for the detection of ∼1 Hz couplings that allows direct identification of N−H:C═O hydrogen bond donors and acceptors in solution through trans hydrogen bond $^{h3}J_{NC'}$ scalar couplings was used.[32] Couplings of ∼15 Hz [$J_{N(i)C(i-1)}$] across the hydrogen bonds are suppressed in the experiment. NMR data were acquired for two separate sets of experiments, each set comprising (a) a reference HNCO experiment and (b) the long-range HNCO hydrogen bond experiment using 24 and 96 scans, respectively. For a hydrogen bond, with a as a donor and b as an acceptor, the size of the $^{h3}J_{NC'}$ coupling constant was calculated quantitatively from cross-peak intensities of the two experiments using eq 5:[32]

$$^{h3}J_{NC'} = [(I_{lr}/I_{ref})(N_{ref}/N_{lr})]^{1/2}/(2\pi T) \quad (5)$$

where I_{lr} is the intensity of the cross-peak in the long-range HNCO experiment, I_{ref} is the intensity of the cross-peak in the reference experiment, N_{ref} is the number of scans used in the reference experiment, and N_{lr} represents the number of scans used in the long-range experiment. The N_{ref}/N_{lr} ratio corrects for the discrepancy in the number of transients averaged per FID in the two experiments. The value of T was set to 66.6 ms in the experiments. The uncertainties in couplings were estimated using eq 6

$$\sigma(^{h3}J_{NC'}) = 0.5(^{h3}J_{NC'})[\{\sigma(I_{lr})\}/(I_{lr})] \quad (6)$$

where σI_{lr} is the uncertainty in intensity, measured as the standard deviation of the signal intensity in a region of the spectrum with no cross-peaks. The scalar coupling constants are extremely sensitive to the N−O atom distance across hydrogen bonds[33−35] and therefore can be converted to hydrogen bond lengths using the empirical relationship (eq 7)[34]

$$R_{NO} = 2.75 - 0.25 \ln(^{h3}J_{NC'}) \pm 0.06 \text{ Å} \quad (7)$$

RESULTS

Ubiquitin is an amazing molecule with numerous binding partners that interact via their structurally diverse motifs. The structural features of ubiquitin that bestow it with this unique ligand diversity remain to be fully understood. Here, we have studied the interaction of ubiquitin with a STAM1 UIM. A ribbon representation of the ubiquitin molecule with the three residues, Ile 44, Val 70, and Leu 8, that form the hydrophobic patch is shown[36] (Figure 1). The UIM binds the ubiquitin molecule in a conformation antiparallel to the β_4 strand as shown[36] [based on Protein Data Bank (PDB) entry 2D3G, crystallization conditions of pH 9.5 and PEG400].

dx.doi.org/10.1021/bi3004268 | Biochemistry 2012, 51, 8111−8124

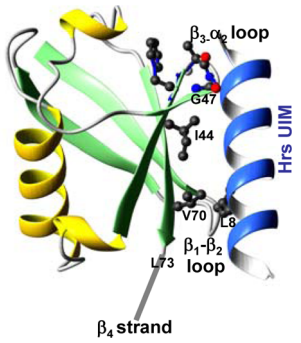

Figure 1. Interaction surface of ubiquitin. A ribbon representation of the three-dimensional structure of ubiquitin, complexed to the hepatocyte growth factor-regulated tyrosine kinase substrate (HRS) UIM (blue). This figure is based on the crystal structure of PDB entry 2D3G, displaying the residues that form the hydrophobic patch as ball and stick. As the ubiquitin molecule extends up to only residue 72 in PDB entry 2D3G, strand β_4 has been extended to mark the position of Leu 73.

Changes in the Backbone Conformation of Ubiquitin upon UIM Interaction. The most commonly used approach for following the changes in the backbone conformation of a protein is following the chemical shift perturbation of its amides upon ligand interaction. In ubiquitin, the amides of Thr 7, Leu 8, Ile 13, Thr 14, Arg 42, Leu 43, Ile 44, Phe 45, Ala 46, Gly 47, Lys 48, Gln 49, Leu 50, Leu 71, Arg 72, and Leu 73 display a significant change in chemical shift upon UIM binding (Figure 2A). Likewise, the backbone nitrogen chemical shifts also display changes for residues Leu 7, Ile 13, Thr 14, Arg 42, Leu 43, Ile 44, Ala 46, Gly 47, Lys 48, Gln 49, Leu 50, Leu 71, and Arg 72 (Figure 2B). The pattern of perturbation was very similar for the CO chemical shifts; Thr 12, Gln 40, Gln 41, Arg 42, Ile 44, Ala 46, Gly 47, Glu 51, Leu 69, and Val 70 display chemical shift changes greater than one standard deviation (Figure 2C). All these results are in sync with the previous studies.[19,37,38]

The amide protons and nitrogen chemical shifts are excellent probes for characterizing the strength of protein−ligand interactions and are widely used to determine K_d values precisely. Therefore, chemical shift changes of the three residues that display large δHN change upon UIM interaction, namely, Ala 46, Gly 47, and Ile 13, were used to determine the strength of the ubiquitin−STAM1 UIM interaction. A K_d value of ~1.79 ± 0.15 mM was calculated for the interaction (Figure 1 of the Supporting Information).

C_α chemical shift changes were also followed for ubiquitin upon complexation with the STAM1 UIM. A large C_α chemical shift change of >1.0 ppm was observed for Ile 45 upon binding to UIM, suggesting major adjustments in the backbone. A few other residues also display chemical shift changes greater than one standard deviation: Thr 7, Leu 8, Thr 9, Glu 24, Gly 47, Leu 69, Leu 71, Arg 72, and Arg 74. The CBCAcoNH spectra of free and UIM-bound ubiquitin are shown, displaying strips for Ala 46 and Lys 48, the two residues that lie close to Ile 44, and display significant changes in the C_α and C_β chemical shifts of Gly 47 and Phe 45 upon UIM binding (Figure 3).

Comparison of the chemical shift changes reported by three different nuclei (δHN, δCO, and δC_α) shows some level of agreement. However, the conformational changes observed at the backbone amides and carbonyls for a few residues, viz., Thr 12, Ile 13, Gln 40, Gln 41, Arg 42, Leu 51, and Gln 62 (Figure 2A of the Supporting Information), are not supported by the C_α chemical shift changes. These amides and carbonyls are

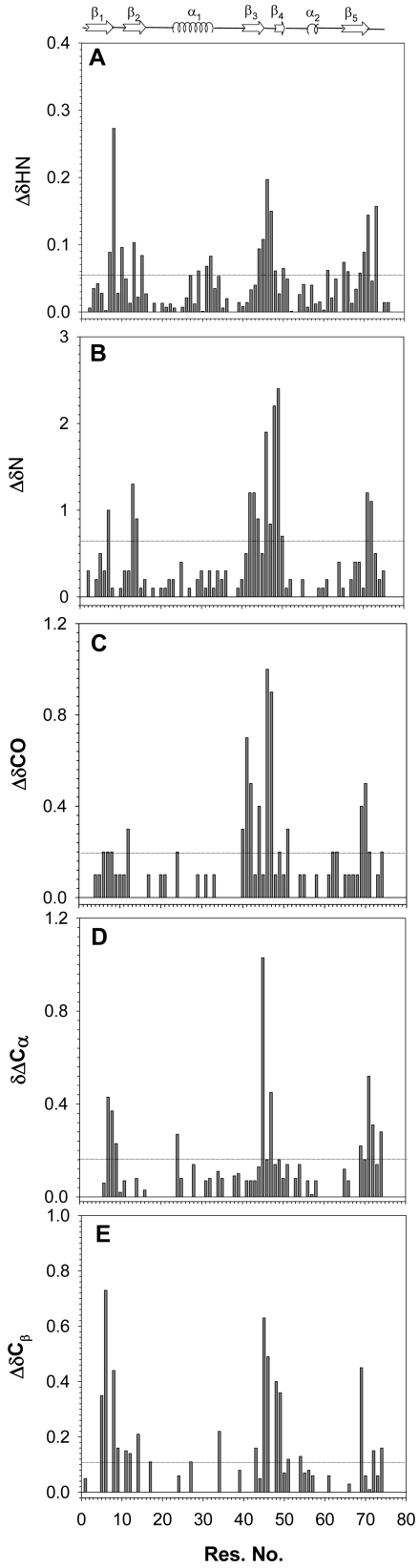

Figure 2. Chemical shift perturbations in ubiquitin upon ligand binding. Changes in (A) δHN, (B) δN, (C) δCO, (D) δC_α, and (E) δC_β chemical shifts as a function of residue number in ubiquitin upon complexation with the UIM of STAM1.

dx.doi.org/10.1021/bi3004268 | *Biochemistry* 2012, 51, 8111−8124

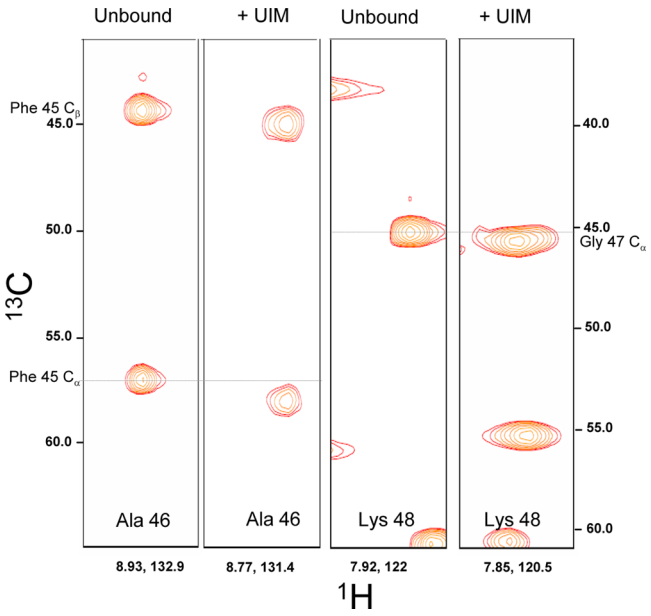

Figure 3. C_α and C_β chemical shift changes in ubiquitin upon UIM binding. Strip plots of the CBCAcoNH spectra of ubiquitin for the amides of Ala 46 and Lys 48 in free and UIM-complexed ubiquitin as marked. The data were processed using nmrPipe and analyzed using Sparky.[23]

localized away from the ligand binding site in ubiquitin (Figure 2B of the Supporting Information), and therefore, the observed changes could be an indirect effect of either a hydrogen bond or through-bond inductive effects. For instance, the arginine 42 side chain has been shown to form a salt bridge with the side chain of Glu 259 of the Hrs UIM in the crystal structure of PDB entry 2D3G,[36] an interaction that could influence the nearby amides of Gln 40 and Gln 41. Similarly, the Ile 13 δHN chemical shift does not interact directly with the ligand but displays a large HN chemical shift change. Amide proton, nitrogen, and carbonyl chemical shifts can be influenced by hydrogen bond interactions and the local environment.[39,40] C_α chemical shifts, on the other hand, are dependent solely on the ϕ and ψ backbone torsion angles[41,42] and, hence, are the most reliable reporters of the backbone conformational change.

Side Chains Experience a Noticeable Change in Conformation. C_β, C_γ, C_δ, and C_ε chemical shift changes report side chain conformation only and, hence, are sensitive probes for following their rearrangements upon ligand binding. C_β chemical shift changes were observed for Val 5, Lys 6, Leu 8, Thr 14, Glu 34, Phe 45, Ala 46, Lys 48, Gln 49, and Leu 69 (Figure 2E), suggesting slight alterations in their side chain orientations. No C_β change was observed for Ile 44.

A remarkable change in the chemical shift was observed for the γ- and δ-carbons of Thr 7, Leu 8, Thr 9, Ile 13, Thr 14, Glu 34, and Ile 44, suggesting changes in the χ_2 and χ_3 angles. In the case of Ile 44, the CG1, CG2, and CD1 atoms change by 1.0, 0.8, and 0.6 ppm, respectively, suggesting slight changes in its side chain conformation. For a few residues, the γ and δ chemical shifts could not be observed in the UIM-bound ubiquitin, namely, Leu 43, Lys 48, Leu 67, Leu 69, Val 70, and Leu 71, probably because of line broadening. Two solvent-exposed side chains also appear to change position as a result of the interaction, Gln 40 and Gln 49, as disclosed from the ^{1}H−^{15}N HSQC spectrum.

Changes in Hydrogen Bond Lengths upon UIM Binding. Trans hydrogen bond scalar couplings provide insights into the dynamic changes in hydrogen bond interactions. As our solution studies suggest a remarkable change in δHN, δCO, and δC_α chemical shifts upon UIM binding, we speculate that the changes could be translated into minor alterations in hydrogen bond lengths. A 1 mM ^{15}N- and ^{13}C-labeled ubiquitin sample expressed in D_2O was used for this study. The protein:ligand ratio was maintained at 1:6 in the UIM-bound ubiquitin sample, and the pH of the sample was adjusted to 6.0. A total of 19 hydrogen bonds could be observed in free ubiquitin at 298 K, and the longest hydrogen bond detected using the long-range HNCO experiment [HN (Asp 32−Ala 28) CO] was 3.04 ± 0.05 Å long. The $^{h3}J_{NC'}$ values for free and UIM-bound ubiquitin from two independent sets of experiments are listed in Table 1. The hydrogen bonds and their precise location in the ubiquitin molecule are illustrated in Figure 4. A quantitative increase in the hydrogen bond lengths was observed for HN (Leu 15−Ile 3) CO, HN (His 68−Ile 44) CO, and HN (Leu 69−Lys 6) CO hydrogen bonds. Hydrogen bonds HN (Ile 44−His 68) CO, HN (Leu 50−Leu 43) CO, and HN (Arg 72−Gln 40) CO displayed a noticeable decrease in length (Figure 4A,B). Upon UIM interaction, the HN (Phe 4−Ser 65) CO hydrogen bond could not be observed in the ubiquitin−UIM complex while there was signal overlap even in free ubiquitin. Hence, the information pertaining to this bond is purely qualitative. Resonances for two hydrogen bonds mutually overlapped in the reference spectrum of the complex, HN (Ile 23−Arg 54) CO and HN (Arg 42−Val 70) CO, and hence, the data for these two bonds have not been analyzed quantitatively. However, qualitatively the HN (Ile 23−Arg 54) CO cross-peak in the long-range experiment displays a marked decrease in intensity, which implies a decrease in coupling and hence an increase in the hydrogen bond length.

Backbone Dynamics Change Remarkably in the Presence of UIM. Correlated slow time scale motions have been shown to be associated with important biological functions, like enzyme catalysis,[43] ligand binding[44,45] etc. To understand the role of slow dynamics in ligand recognition by ubiquitin (observable at the amides of Ile 23, Asn 25, Thr 55, and Val 70 in free ubiquitin), relaxation experiments were conducted with ubiquitin complexed to the UIM at 278 K as illustrated in Figure 5. Relaxation studies were conducted at low temperatures in particular to shorten the time scales of the exchange processes so that they fall within the CPMG time scale.[46−48] The window of conformational change suitable for detection by CPMG experiments is ≤2000 s^{-1} because of limitations in the maximal radiofrequency field that can be applied in a relaxation experiment.

A complex with a 1:6 ubiquitin:UIM ratio was prepared using a 2 mM ubiquitin solution in 50 mM sodium phosphate buffer, with the final pH of the complex adjusted to 6.0. A dotted line in Figure 1 of the Supporting Information indicates the working concentration of ubiquitin and the ligand used in our relaxation experiments. At these concentrations, ubiquitin is still not completely bound; the fraction bound is ∼0.95. Assuming that K_{on} is diffusion-limited on rate, independent of the system,[49] ∼1 × 10^8 M^{-1} s^{-1}, and using a K_d value of 1.79 mM that we calculated experimentally, K_{off} would be ∼1.7 × 10^5 s^{-1}. Using the relationship for fast exchange ($k_{ex} = k_{on}$[ligand] + k_{off}) and a final ligand concentration of 12 mM, the k_{ex} for the association−dissociation kinetics would be 1.37 × 10^6 s^{-1}. Notably, the rate of dissociation of ubiquitin from the UIM is

dx.doi.org/10.1021/bi3004268 | Biochemistry 2012, 51, 8111−8124

Table 1. Coupling Constants and Hydrogen Bond Lengths in Free Ubiquitin and Ubiquitin Complexed to the STAM1 UIM

	free ubiquitin		UIM-bound ubiquitin			
HN−CO hydrogen bond	$^{h3}J_{NC'}$ (Hz)	d_{H-N} (Å)	$^{h3}J_{NC'}$ (Hz)	d_{H-N} (Å)	Δ (Å)	effect
K6−L67	0.59 ± 0.00[a]	2.88	0.58 ± 0.01[a]	2.88	0	–
	0.59 ± 0.01[a]		0.61 ± 0.02[a]			
T7−K11	0.61 ± 0.01[a]	2.87	0.59 ± 0.01[a]	2.89	−0.02	–
	0.61 ± 0.00[a]		0.57 ± 0.02[a]			
I13−V5	0.69 ± 0.03[a]	2.85	0.73 ± 0.01[a]	2.83	0.02	–
	0.68 ± 0.01[a]		0.76 ± 0.01[a]			
L15−I3	0.66 ± 0.01[a]	2.86	0.56 ± 0.02[a]	2.89	−0.03	stretch
	0.64 ± 0.02[a]		0.58 ± 0.04[a]			
V17−M1	0.69 ± 0.02[a]	2.84	0.65 ± 0.01[a]	2.86	−0.02	–
	0.70 ± 0.01[a]		0.66 ± 0.02[a]			
I23−R54	0.58 ± 0.01[a]	2.89	ND[b]	ND[b]	ND[b]	–
	0.56 ± 0.03[a]					
Q31−K27	0.43 ± 0.01[a]	2.97	0.44 ± 0.03[a]	2.95	0.02	–
	0.42 ± 0.03[a]		0.47 ± 0.02[a]			
D32−A28	0.30 ± 0.01[a]	3.04	0.33 ± 0.01[a]	3.04	0	–
	0.32 ± 0.04[a]		0.31 ± 0.03[a]			
R42−V70	0.47 ± 0.02[a]	2.95	ND[b]	ND[b]	ND[b]	–
	0.45 ± 0.03[a]					
I44−H68	0.65 ± 0.02[a]	2.87	0.78 ± 0.03[a]	2.81	0.06	shrink
	0.62 ± 0.01[a]		0.81 ± 0.02[a]			
F45−K48	0.42 ± 0.01[a]	2.97	0.45 ± 0.03[a]	2.95	0.02	–
	0.41 ± 0.02[a]		0.47 ± 0.03[a]			
L50−L43	0.55 ± 0.00[a]	2.91	0.64 ± 0.01[a]	2.87	0.04	shrink
	0.53 ± 0.01[a]		0.62 ± 0.01[a]			
S57−P19	0.43 ± 0.02[a]	2.97	0.43 ± 0.02[a]	2.95	−0.02	–
	0.42 ± 0.02[a]		0.46 ± 0.04[a]			
F4−S65	ND[b]	ND[b]	ND[b]	ND[b]	ND[b]	–
L67−F4	0.59 ± 0.02[a]	2.89	0.60 ± 0.01[a]	2.89	0	–
	0.57 ± 0.01[a]		0.58 ± 0.01[a]			
H68−I44	0.82 ± 0.02[a]	2.8	0.72 ± 0.01[a]	2.84	−0.04	stretch
	0.84 ± 0.01[a]		0.70 ± 0.01[a]			
L69−K6	0.41 ± 0.01[a]	2.97	0.39 ± 0.02	3	−0.03	stretch
	0.41 ± 0.02[a]		0.37 ± 0.03			
V70−R42	0.72 ± 0.01[a]	2.83	0.75 ± 0.01[a]	2.82	0.01	–
	0.73 ± 0.02[a]		0.78 ± 0.04[a]			
R72−Q40	0.36 ± 0.01[a]	3	0.49 ± 0.02[a]	2.92	0.08	shrink
	0.38 ± 0.01[a]		0.52 ± 0.02[a]			

[a]Values for $^{h3}J_{NC'}$ couplings calculated from two separate data sets, acquired independently. [b]The $^{h3}J_{NC'}$ trans hydrogen bond couplings and hydrogen bonds were not detected because of spectral overlap in the reference spectrum.

quite high, maintaining a high turnover rate that might be relevant in its biological function.

Despite the fairly weak nature of the ubiquitin−UIM interaction, we were able to follow the changes in the dynamics of ubiquitin upon interaction with the UIM. Overall, the peaks were slightly broader in the complex than in free ubiquitin. The relaxation parameters for free ubiquitin as well as ubiquitin complexed to a UIM of STAM1 are compared (Figure 5). R_1 relaxation rate constants obtained using the inversion−recovery profiles were slightly lower than those of free ubiquitin (Figure 5A). Interestingly, unlike the case in free ubiquitin, in which Ile 23, Asn 25, Thr 55, and Val 70 display high R_2 values compared to those of the rest of the amides, in the UIM-bound ubiquitin, high R_2 values were observed for only Ile 23 (Figure 5B). On the other hand, a few other residues display high R_2 values in the complex, viz., Thr 7, Ile 13, Thr 14, Gln 41, Leu 43, Ile 44, Gly 47, Lys 48, Gln 49, His 68, and Leu 69. An overall increase in the average relaxation rate (R_2) was observed compared to that of free ubiquitin. Steady state $^{15}N\{^1H\}$ NOE experiments conducted with and without ^1H saturation were used to determine the NOE values (Figure 5C). No major differences could be observed between free and UIM-bound ubiquitin with regard to the NOE values.

The raw relaxation data were fit to the extended model free formalism developed by Lipari and Szabo[50] using FAST-Modelfree.[29] An axially symmetric model of the diffusion tensor was used for analyzing the relaxation data for free as well as UIM-complexed ubiquitin. Models with the fewest parameters that gave a statistically significant χ^2 value were selected. Residues that showed significant resonance overlap were excluded from the analysis. These include Leu 15, Glu 16, Val 26, Arg 42, Leu 50, Arg 72, and Arg 74. In addition, Ala 46 was extremely broadened at 278 K in the ubiquitin−UIM complex and hence was not included in the analysis. The observed rotational correlation time was ∼14.14 ns for ubiquitin complexed to the UIM, much longer than that of free ubiquitin (9.62 ns) at 278 K, reflecting an increase in the size of the complex. Order parameters obtained from the model

dx.doi.org/10.1021/bi3004268 | Biochemistry 2012, 51, 8111−8124

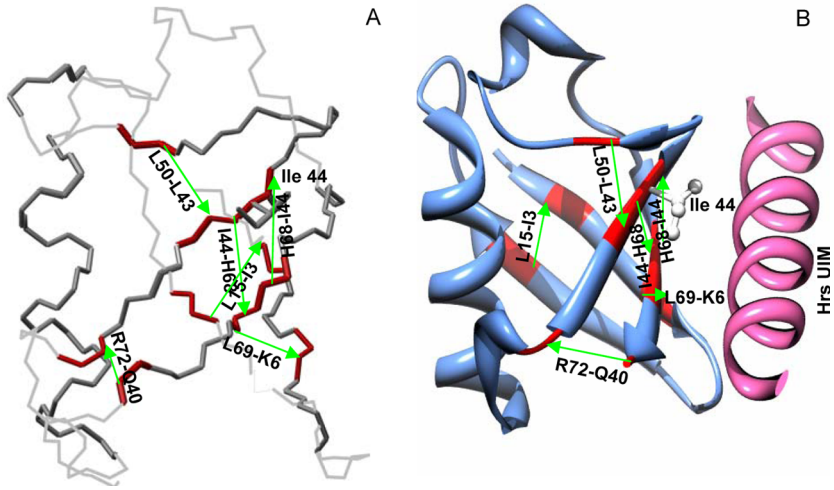

Figure 4. Changes in the backbone hydrogen bond lengths upon UIM binding. (A) Ubiquitin molecule (backbone) with the residues forming hydrogen bonds colored red. The direction of the green arrow marks the direction of the hydrogen bond, i.e., donor → acceptor. (B) Ribbon representation of the ubiquitin molecule complexed to the Hrs UIM displaying the hydrogen bonds experiencing changes in length upon UIM interaction (green).

free analysis have been plotted as a function of residue number for both free and UIM-complexed ubiquitin (Figure 5D). It is noteworthy that some of the residues that form the binding interface (residues Ile 44−Asp 58) display a slight decrease in order parameter upon UIM binding, suggesting an increase in backbone flexibility. The R_{ex} parameter that reports microsecond to millisecond time scale fluctuations (a larger value corresponding to greater conformational heterogeneity) is also shown for each residue (Figure 5E). In the UIM-complexed ubiquitin, a few residues in addition to Asn 25 require the R_{ex} term. These include Thr 7, Ile 13, Leu 43, Ile 44, Gly 47, Lys 48, and Gln 49. Line broadening observed at the amides of Glu 24 and Gly 53 in free ubiquitin remains unaltered in the complex, implying that the side chain to backbone hydrogen bond [CO (Glu 24−Gly 53) NH] reported by two recent studies is intact in the complex.[46,51]

^{15}N constant-time CPMG relaxation dispersion experiments that provide a quantitative measure of the exchange rates were also conducted with free ubiquitin, as well as ubiquitin complexed to UIM, at 278 K on a 700 MHz NMR spectrometer. Individual fits to the dispersion profiles using NESSY[30] are shown for residues that display nonflat dispersion profiles in free ubiquitin and some of the residues in ubiquitin complexed to UIM (Figure 6B). In free ubiquitin, only Ile 23, Asn 25, Thr 55, and Val 70 display noticeable conformational exchange at 278 K. Global fitting of the dispersion profiles of these four residues gave an exchange rate of 2.6×10^4 s^{-1}, fairly close to the values reported previously.[47] However, in ubiquitin complexed to the UIM, a large number of residues displayed conformational exchange. This experiment in fact identified several more residues that were not observed in the R_2 relaxation experiments. Of the four residues that display dynamics in free ubiquitin, only two display conformational exchange upon binding to the UIM, i.e., Asn 25 and Val 70, with a noticeable change in the R_2^{eff}. A total of 22 residues could be fit to a two-state slow exchange process using the Carver and Richards equation[31] in UIM-complexed ubiquitin, viz., Lys 6, Thr 7, Thr 14, Leu 15, Asn 25, Glu 34, Gln 41, Arg 42, Leu 43, Phe 45, Gly 47, Lys 48, Leu 50, Ser 57, Glu 64, Ser 65, Leu 67, His 68, Leu 69, Val 70, Leu 71, and Leu 73. Ala 46 that displayed maximal amplitude motions was excluded from the analysis because of extreme line broadening observed at lower CPMG frequencies used in our relaxation dispersion experiments. The exchange rate (k_{ex}), the population of the exchanging species, and the chemical shift change deduced from the relaxation dispersion experiments are listed in Table 2. Relatively large $\Delta\delta_{NCPMG}$ changes were observed for Thr 7, Thr 14, Arg 42, Leu 43, Lys 48, Leu 50, Leu 71, and Leu 73 in UIM-complexed ubiquitin, in sync with our chemical shift mapping studies. Notably, most of the residues displaying conformational exchange are similar to those mentioned in a previous study of a ubiquitin−UIM fusion protein.[8] A comparatively higher R_2^{eff} was observed for Gly 47 and Lys 48. The amplitude of the dispersion profile was also remarkably different for these two residues in UIM-complexed ubiquitin (Figure 6B). Global fitting of approximately 72% of the residues was achieved using model 3, viz., Lys 6, Thr 7, Thr 14, Asn 25, Glu 34, Gln 41, Arg 42, Leu 43, Phe 45, Gly 47, Lys 48, Leu 50, Glu 64, Leu 67, Leu 69, and Val 70, to yield an exchange rate of ∼3505 ± 6 s^{-1}, suggesting concerted motions, with an exchanging population p_b of 0.12 ± 0.01. Converting the global fit exchange rate k_{ex} to the forward and reverse rate constants [assuming the process is (ground state) A ↔ B (excited state)] gave a forward exchange rate of ∼421 s^{-1} and a B → A reverse rate of 3084 s^{-1}. Some residues that displayed a nonflat dispersion profile and could not be fit to the global exchange process were Leu 15, Ser 65, His 68, Leu 69, Leu 71, and Leu 73. Table 3 compares the exchange rates (k_{ex}) observed in free ubiquitin as well as ubiquitin complexed to the UIM at 278 K.

While most of the residues display millisecond motions in ubiquitin upon UIM binding, several residues also experience extremely fast dynamics and could be fit to only model 2 using NESSY.[30] These include residues Ile 13, Ile 23, Asp 39, Ile 44, Gln 49, and Thr 55, displaying k_{ex} values in the range of 3000−10000 s^{-1}.

Intermolecular NOEs between the Amides of Ubiquitin and the UIM Side Chains. ^{13}C−^{15}N-filtered, ^{15}N-edited NOESY experiments were conducted to identify the amides in ubiquitin that interact directly with the UIM peptide in solution. Conceivably, only four backbone amides of ubiquitin make significantly close contacts of <5 Å with the STAM1 UIM side chains. These include the amides of Ala 46, Gly 47, Lys 48,

dx.doi.org/10.1021/bi3004268 | *Biochemistry* 2012, 51, 8111−8124

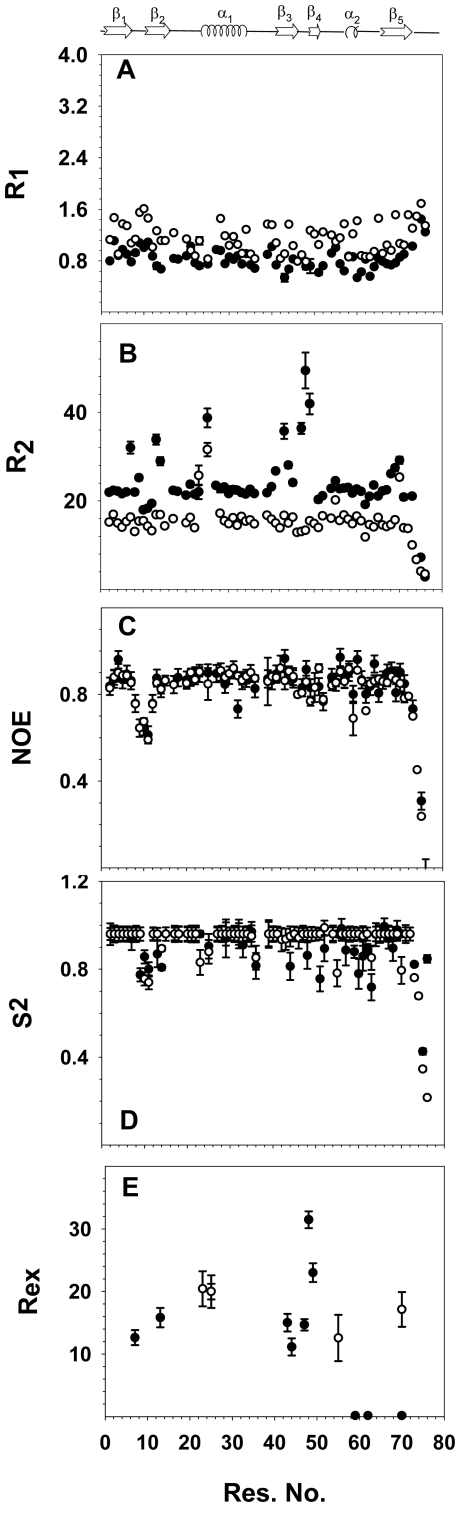

Figure 5. ^{15}N relaxation parameters for free ubiquitin and ubiquitin complexed to the UIM. Plots of (A) R_1, (B) R_2, (C) NOE, (D) model free parameter S^2, and (E) model free parameter R_{ex} obtained by fitting the raw data to the extended Lipari–Szabo model free formalism as described in Experimental Procedures for free (○) and UIM complexed (●) ubiquitin. Errors are represented as error bars. The overall molecular tumbling correlation time for wild-type ubiquitin was determined to be 9.6 ± 0.2 ns and that for the ubiquitin–UIM complex 14.14 ± 0.5 ns at 278 K.

and Leu 73 as shown in panels A–C and E of Figure 7. The first three residues form a contiguous patch in the structure of ubiquitin and display NOEs to the H_β atom of Ser 183 and the H_β and H_δ atoms of Leu 184 of the STAM1 UIM. Likewise, leucine 73, localized in strand β_4, shows a NOE to the H_γ atom of Glu 172 of the STAM1 UIM. Apart from the backbone amides, the side chain of Gln 49 is also found close to the H_δ atom of Leu 184 as revealed by the NOE data (Figure 7D). The observed NOEs are consistent with the presence of side chain to backbone hydrogen bonds between the Ser of UIM and Ala 46/Gly 47 of ubiquitin as well as the Glu side chain of UIM and the Leu 73 amide of ubiquitin.

Insights from the Crystal Structures of Ubiquitin Complexes. A large number of crystal structures of the noncovalent complexes of ubiquitin are available in the Protein Data Bank, with a wealth of information still unexplored. Superposition of the available X-ray structures and comparison with our NMR results allowed us to draw inferences pertaining to the ubiquitin–UIM interaction. An overlay of the crystal structures of ubiquitin complexes with a resolution of 2.6 Å or better is shown in Figure 8A. Notably, in the crystal structures, the β_1–β_2 loop (Figure 8C) displays two distinct conformations for the backbone (colored blue) and side chains (colored green), markedly different from each other. Likewise, the ubiquitin backbone close to Val 70 in strand β_4 (Figure 8D) and the β_3–α_2 loop (Figure 8B) also show some differences in conformation in the different structures.

To gain a comprehensive view of the major changes occurring in ubiquitin as a result of UIM interaction, the regions displaying NOEs to the UIM peptide (Figure 9A), C_α chemical shift changes (Figure 9B), millisecond motions (Figure 9C), and changes in hydrogen bond lengths (Figure 9D) have been mapped onto the surface of ubiquitin and compared with the regions displaying conformational heterogeneity in the crystal structures of ubiquitin complexes (Figure 9E). Unquestionably, the ubiquitin–UIM interaction involves major changes (in backbone as well as dynamics) at primarily three sites, the β_1–β_2 loop, the β_3–α_2 loop, and strand β_4. Excellent agreement could be observed between the C_α conformational changes and the structural variations observed in the crystal structures of ubiquitin complexes. Likewise, a good overlap was observed between the regions displaying millisecond motions and the changes in hydrogen bond lengths.

For quantitative comparisons, changes in C_α and C_β chemical shifts were predicted for all the residues present in the two ubiquitin molecules (chain ID A and chain ID B), bound to the Hrs UIM in PDB entry 2D3G, as well as free ubiquitin in PDB entry 1UBQ using SPARTA+.[52] As illustrated in Figure 3 of the Supporting Information, some level of disparity exists between the two molecules present in PDB entry 2D3G with regard to the predicted C_α and C_β chemical shift changes, suggesting slight differences in their interaction with ubiquitin. Residues that display relatively large C_α and C_β chemical shifts in our NMR chemical shift mapping studies have been highlighted (Figure 3A,B of the Supporting Information). Overall, good agreement was observed between the experimentally observed chemical shifts and the predicted C_α chemical shift differences for residues Thr 7, Leu 8, Glu 24, Phe 45, Gly 47, and Leu 71 (Figure 3A of the Supporting Information). Lys 6 and Leu 69 display an excellent correlation between the experimental and predicted C_β chemical shift changes (Figure 3B of the Supporting Information). The experimentally determined C_β chemical shifts for Val 5, Leu 8, Lys 11, Leu 14, Glu 34, Gln 49, and Arg 54 are in close agreement with the predicted chemical shifts.

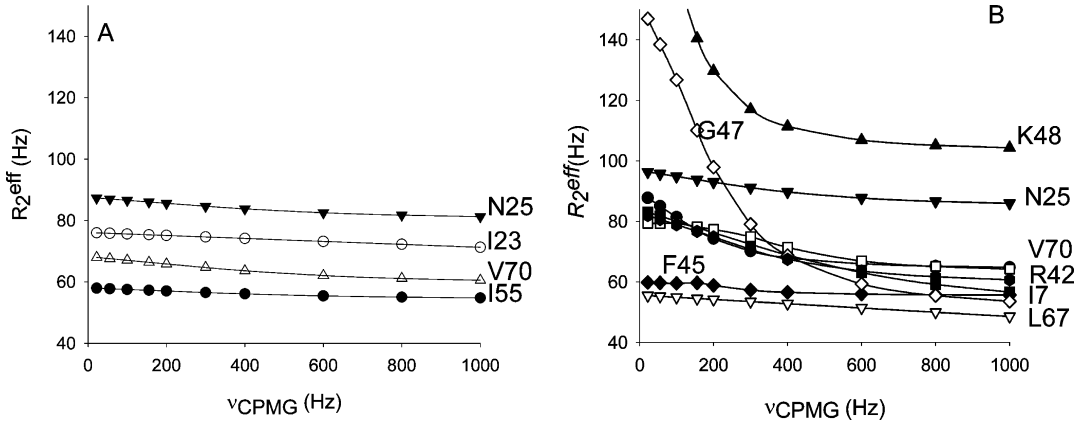

Figure 6. Analysis of the ^{15}N relaxation dispersion experiments. ^{15}N constant-time relaxation dispersion profiles for residues in (A) free ubiquitin and (B) some of the residues in ubiquitin complexed to UIM at 278 K on a 700 MHz NMR spectrometer. The data were processed using nmrPipe[22] and analyzed using Sparky[23] and NESSY.[30]

Table 2. Physical Parameters Obtained by Fitting the ^{15}N Relaxation Dispersion Profiles of Individual Residues to a Two-State Slow Exchange Process Using eq 3

residue	k_{ex} (s^{-1})	p_b (%)	$\Delta\delta\omega_{NCPMG}$ (ppm)	$\Delta\delta_N$[a] (ppm)
Lys 6	3000 ± 321	2	2.39 ± 1.02	0.3
Thr 7	1155 ± 130	16	1.10 ± 0.31	1.0
Thr 14	919 ± 142	2	3.52 ± 0.13	0.9
Leu 15	157 ± 80	7	3.52 ± 0.06	0.1
Asn 25	2547 ± 509	30	0.86 ± 0.41	0.4
Glu 34	3000 ± 261	15	0.75 ± 0.42	0.3
Gln 41	27 ± 18	30	2.28 ± 0.16	0.5
Arg 42	3449 ± 208	16	2.13 ± 0.70	1.2
Leu 43	56 ± 50	30	5.90 ± 0.24	1.2
Phe 45	15 ± 6	30	3.87 ± 0.34	0.5
Gly 47	1147 ± 339	19	2.26 ± 0.44	0.8
Lys 48	791 ± 275	30	1.49 ± 0.22	2.2
Leu 50	104 ± 82	5	3.66 ± 0.24	0.7
Ser 57	3000 ± 175	9	0.84 ± 0.59	0.0
Glu 64	803 ± 160	2	2.24 ± 0.25	0.4
Ser 65	52 ± 30	6	2.49 ± 0.38	0.1
Leu 67	3365 ± 1000	6	4.85 ± 2.12	0.2
His 68	2753 ± 321	30	0.78 ± 0.74	0.4
Leu 69	970 ± 196	3	3.15 ± 0.19	0.4
Val 70	1836 ± 355	5	2.63 ± 0.66	0.1
Leu 71	16 ± 32	29	2.96 ± 0.19	1.2
Leu 73	831 ± 177	1	3.14 ± 0.17	1.1

[a]Changes in the $\Delta\delta_N$ chemical shift of ubiquitin upon binding to the UIM in a $^1H-^{15}N$ HSQC experiment.

Table 3. Rate Constants Observed for the Global Exchange Processes Observed in Free Ubiquitin and Ubiquitin Complexed to the UIM at 278 K

	rate constant	^{15}N relaxation dispersion (s^{-1})	p_b[a] (%)
free ubiquitin	k_{ex}	2.6×10^4	7.3
ubiquitin−UIM complex	k_{ex}	3505 ± 6	12

[a]Population of the exchanging species.

As some of the hydrogen bonds display significant changes in lengths upon UIM binding in our study, the lengths of all the backbone to backbone hydrogen bonds in the 29 PDB entries of ubiquitin complexes were determined using Chimera.[53] Interestingly, a slight variation in length was observed for most of the hydrogen bonds, highlighting the intrinsic flexibility of the ubiquitin backbone (Figure 4 of the Supporting Information). The distances shown in the figure are between the donor atom (N) and the acceptor atom (O). The least perturbed hydrogen bonds were as follows: N (I30−V26) CO, N (E34−I30) CO, N (L67−F4) CO, N (K6−L67) CO, N (I44−H68) CO, N (L56−D21) CO, N (K27−I23) CO, N (H68−I44) CO, N (V70−R42) CO, N (Q31−K27) CO, and N (L15−I3) CO (standard deviation of ≤0.1). Mapping these residues on the crystal structure of ubiquitin suggests that most of these residues participating in the hydrogen bonds comprise the hydrophobic core. The remaining hydrogen bonds display relatively large deviations reflecting a high level of flexibility. The N (Arg 42−Val 70) CO and N (Arg 72−Gln 40) CO hydrogen bonds displayed the maximal standard deviation, followed by the N (T7−K11) CO hydrogen bond.

DISCUSSION

Ubiquitin's main function is to identify a diverse range of domains and/or motifs present on the surface of its binding partners and covalently modify them to regulate a range of cellular activities. Interestingly, the molecule itself experiences remarkable changes in structure and dynamics during this process, which plausibly holds the key to its unusual ligand diversity.

A major achievement of this study is the observation of backbone C_α conformational changes at three distinct sites in ubiquitin upon UIM interaction, precisely, the residues adjoining Leu 8, Gly 47, and Leu 71. A strong correlation is observed between the residues displaying C_α chemical shift changes and the amides displaying NOEs to the peptide in the $^{13}C-^{15}N$-filtered, ^{15}N-edited experiments, viz., (a) the patch of Ala 46, Gly 47, and Lys 48 and (b) Leu 73, relating conformational change to ligand binding. A noticeable C_α chemical shift change of >1 ppm was observed for Ile 45, and a concomitant change in Gly 47 of ∼0.45 ppm. Though in this study we report the interaction of ubiquitin with the STAM1 UIM only, we performed similar studies in parallel with the hepatocyte growth factor-regulated tyrosine kinase substrate (Hrs) UIM (Ace-QEEEELQLALALSQSEAEEK-NH_2) as well, and the C_α chemical shift changes observed upon UIM binding were precisely the same. Trans hydrogen bond scalar coupling experiments suggest changes in the length

dx.doi.org/10.1021/bi3004268 | Biochemistry 2012, 51, 8111−8124

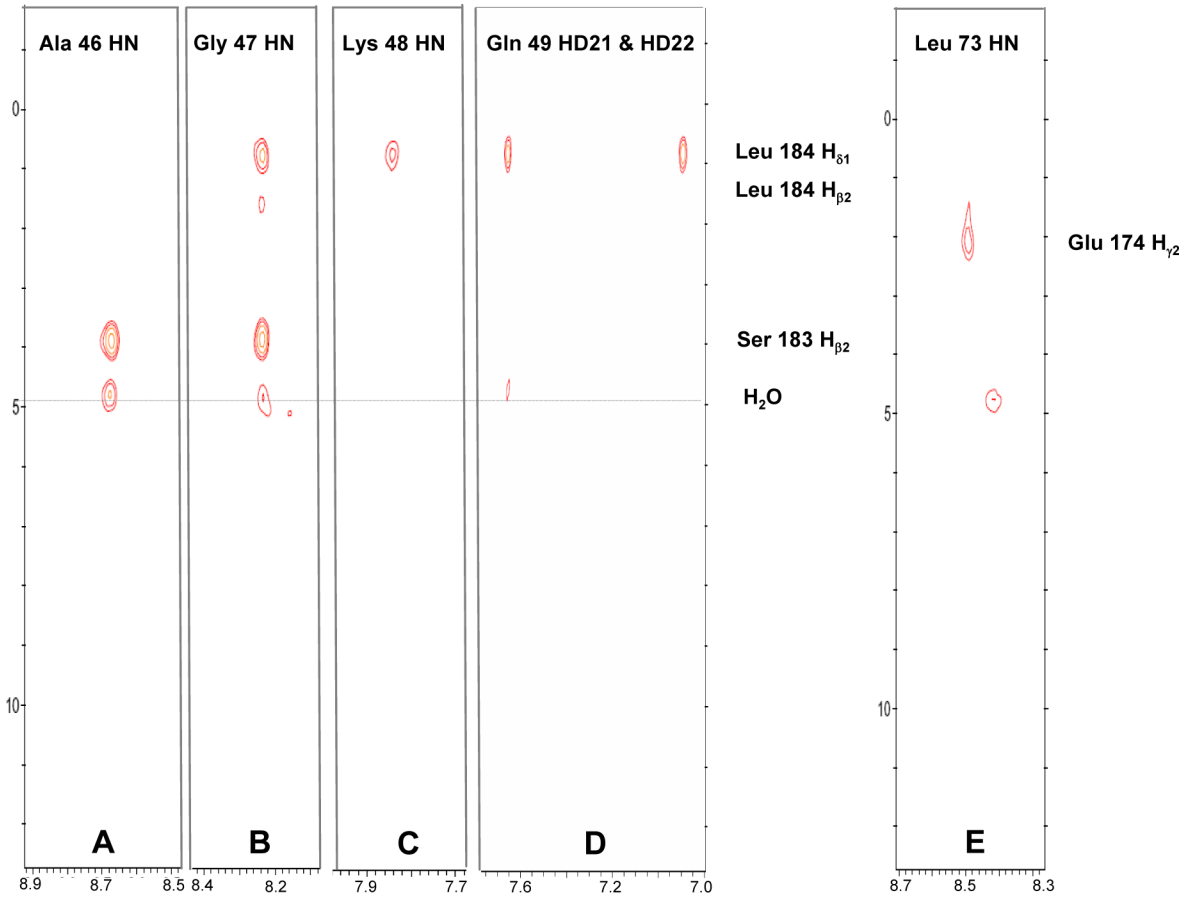

Figure 7. $^{13}C-^{15}N$-filtered, ^{15}N-edited NOESY spectra of ubiquitin complexed to the STAM1 UIM. Strip plots for (A) Ala 46 HN, (B) Gly 47 HN, (C) Lys 48 HN, (D) Gln 49 NH_2, and (E) Leu 73 HN groups displaying NOEs to the side chains of residues in the UIM. The data were processed using nmrPipe[22] and analyzed using Sparky.[23]

of the HN (L50−L43) CO hydrogen bond that lies at the two ends of the $\beta_3-\alpha_2$ loop. In light of the crystal structures of ubiquitin complexes that display a slight forward movement of the $\beta_3-\alpha_2$ loop upon ligand binding, we speculate that the C_α chemical shift change and the change in hydrogen bond length both report the same event. Filtered NOESY experiments lend support to the presence of the Ser 183 H_β atom in the vicinity of Ala 46 and Gly 47 amides, suggesting that the side chain to backbone hydrogen bond, between Ser 183 of the UIM and Gly 47 of ubiquitin (as observed in other studies), is probably the driving force.[54] Presumably, the hydrogen bond draws Gly 47 closer to the ligand, giving rise to the conformational change in the backbone of Gly 47, and a reciprocal change in the conformation of Phe 45. The C_α and C_β chemical shifts of Phe 45 display a constant change upon UIM binding, also supporting this proposition. Prior mutagenesis studies have highlighted the indispensable role of Gly 47 in ubiquitin interactions.[54] Conceivably, a glycine at position 47 performs twofold functions: (a) making the backbone accessible for formation of hydrogen bonds with the ligand and (b) imparting flexibility to the loop so that it can undergo necessary conformational changes in response to the binding and release of the ligand.[55] Knowledge of such structural determinants might be of significance in drug design, to competitively block the ubiquitin binding domains if required.

Apart from the Ala 46-Gly 47 cluster, two other sites [(a) Leu 69, Leu 71, and Arg 72 and (b) Thr 7, Leu 8, and Thr 9] display considerable C_α chemical shift changes upon binding to the UIM. The changes in lengths of HN (Leu 69−Lys 6) CO and HN (Arg 72−Gln 40) CO hydrogen bonds in our study are in compliance with the backbone C_α changes. On the basis of the crystal structures of ubiquitin complexes, we speculate that the conformational change involves upward twisting of strand β_4 and the $\beta_1-\beta_2$ loops. The observation of an NOE between the Glu 174 $H_{\gamma 2}$ atom of the UIM and the Leu 73 amide of ubiquitin conforms with a side chain to backbone hydrogen bond between the two residues, as observed in other studies[56] and in PDB entries 1WR6, 1P3Q, 2IBI, and 3LDZ. Perhaps the intermolecular hydrogen bond plays a pivotal role in the conformational change. The UIM peptide does not seem to make any direct contacts with the amides of the $\beta_1-\beta_2$ loop though. We surmise that the conformational changes observed in the $\beta_1-\beta_2$ loop are primarily induced by the hydrophobic interactions mediated by the side chain of Leu 8 that pulls the backbone closer to the ligand.

Another exciting observation is the striking change in the dynamics of ligand-bound ubiquitin. In a prior study of free ubiquitin, four amides were identified to display slow motions,[46] viz., Ile 23, Asn 25, Thr 55, and Val 70. However, in UIM-complexed ubiquitin, of those four residues, only Asn 25 and Val 70 display those motions, and the R_2^{eff} was much higher for these two residues than for free ubiquitin, suggesting a marked change in the overall intrinsic dynamics upon formation of the UIM complex. It certainly does not imply that the slow motions observed in free ubiquitin are quenched in the complex. Presumably, another exchange process with a much

dx.doi.org/10.1021/bi3004268 | *Biochemistry* 2012, 51, 8111−8124

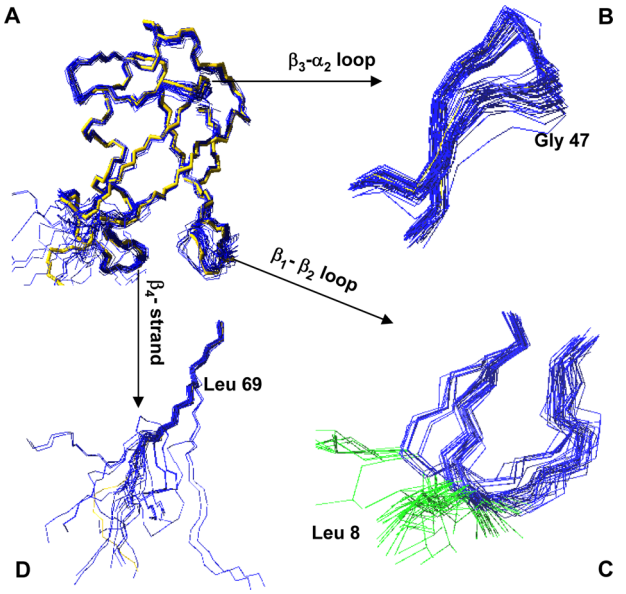

Figure 8. Backbone variations in the crystal structures of ubiquitin complexes. (A) Overlay of the ubiquitin backbones in the crystal structures of ubiquitin complexes, viz., PDB entries 3A33, 2C7N, 2ZNV, 2D3G, 3K9O, 2IBI, 2QH0, 3A1Q, 1WR6, 3CMM, 3COR, 3BY4, 3OJ3, 3IFW, 3PT2, 3I3T, 3A9J, and 3A9K. The conformation of free ubiquitin based on the crystal structure of PDB entry 1UBQ is represented as a yellow strand. The three regions that display a high level of disparity in the X-ray complexes, (B) the β_3–α_2 loop, (C) the β_1–β_2 loop (the side chain of Leu 8 is colored green), and (D) strand β_4, are shown separately. This figure was prepared using Molmol.[61]

larger amplitude becomes the dominating exchange process, as the line broadening observed at the Glu 24 and Gly 53 amides can still be observed in the complex. Interestingly, some of the amides that interact directly with the UIM (based on our C_α chemical shift perturbation study and hydrogen bond experiments) display motions with relatively large amplitudes, viz., Ala 46, Gly 47, and Lys 48, associating ligand binding with the change in dynamics. The maximal amplitude of the dynamics is observed at the Ala 46 amide as we were unable to analyze the residue because of line broadening at lower CPMG frequencies. Only 72% of the residues displaying a nonflat dispersion profile could be fit to one single exchange rate, suggesting the possibility of more than one distinct exchange process in UIM-bound ubiquitin. Most of the residues that could not be fit to the global exchange process lie at the C-terminus of ubiquitin.

On the basis of the crystal structure of PDB entry 2D3G, only two amides in ubiquitin directly interact with UIM side chains, Gly 47 and Leu 73, both involved in a hydrogen bond interaction. It is tempting to speculate that the two hydrogen bonds possibly give rise to two separate conformational exchange processes, one centered at the Ala 46/Gly 47 HN group and the other at the Leu 73 HN group. In a prior study involving the ubiquitin–UIM (Vps27) fusion protein, the authors observed similar slow backbone motions with very similar exchange rates.[8] However, there are a few notable differences. (a) The authors used an F45W mutant of ubiquitin instead of the wild type. (b) A fusion protein of ubiquitin with a linker connecting the UIM was used instead of free UIM. (c) Experiments were conducted at 298 K. Nevertheless, both studies highlight the highly unusual feature of the ubiquitin backbone, i.e., enhanced dynamics upon ligand binding, irrespective of the state of ubiquitin (free or fused).

Some very interesting facts also emerged from our study with regard to the hydrogen bond lengths in the crystal structures of the ubiquitin complexes; the N (Arg 42–Val 70) CO and N (Arg 72–Gln 40) CO hydrogen bonds are maximally perturbed in the crystal structures. The latter hydrogen bond was perturbed in several of the crystal structures we analyzed, leading us to conclude that the N (Arg 42–Val 70) CO hydrogen bond marks the onset of the flexible C-terminus. The N (Val 70–Arg 42) CO hydrogen bond is relatively rigid in contrast. Apart from the three hydrogen bonds mentioned above that display high standard deviations, the N (Lys 29–Asn 25) CO, N (Lys 48–Phe 45) CO, N (Glu 64–Gln 2) CO, N (Val 17–Met 1) CO, N (Ser 65–Gln 62) CO, N (Lys 33–Lys 29) CO, and N (Ser 57–Pro 19) CO bonds also display a high level of variation among the 66 ubiquitin molecules. Thus, an important conclusion that stems from this analysis is that most if not all the hydrogen bonds in ubiquitin are capable of changing length in response to ligand binding (Figure 4 of the Supporting Information). Most interesting of all is the observation that the hydrogen bonds remote from the ligand binding site also display a noticeable disparity in lengths in the different structures of ubiquitin complexes we analyzed, viz., N (Lys 33–Lys 29) CO (Figure 4AC of the Supporting Information), N (Ser 57–Pro 19) CO (Figure 4AD of the Supporting Information), and N (Ile 13–Val 5) CO (Figure 4X of the Supporting Information), suggesting that a conformational change in ubiquitin is facilitated by changes in hydrogen bond lengths all over the protein backbone.

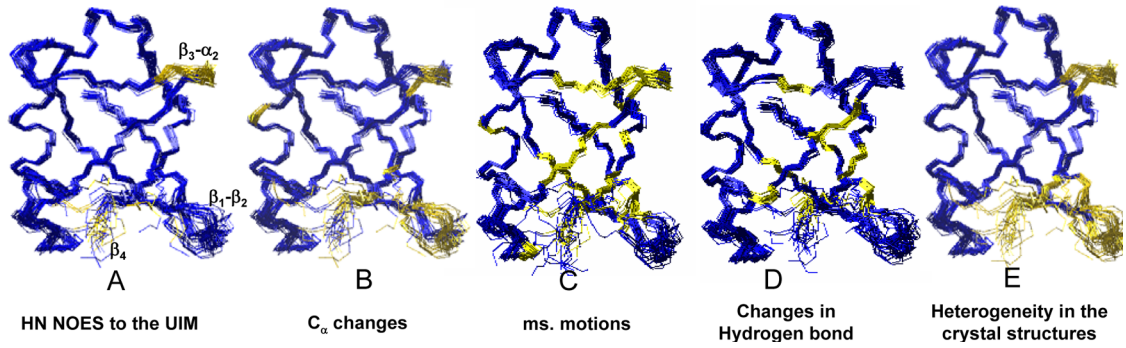

Figure 9. Comprehensive view of the changes occurring in ubiquitin upon ligand binding. Residues of ubiquitin displaying (A) NOEs to the UIM peptide, (B) significant C_α changes upon UIM binding, (C) millisecond motions upon UIM binding, and (D) heterogeneity in the crystal structures of ubiquitin complexes are colored yellow. This figure was prepared using Molmol.[58]

dx.doi.org/10.1021/bi3004268 | *Biochemistry* 2012, 51, 8111–8124

The observations made from the crystal structures were experimentally confirmed from our $^{h3}J_{NC'}$ trans hydrogen scalar coupling experiments. When the UIM binds, the maximally perturbed hydrogen bond was the HN (Arg 72−Gln 40) CO bond in sync with the crystal structures of ubiquitin complexes. The HN (Ile 44−His 68) CO, HN (Leu 50−Leu 43) CO, and HN (Arg 42−Gln 40) CO hydrogen bonds become shorter, while the HN (Leu 15−Ile 3) CO, HN (His 68−Ile 44) CO, and HN (Leu 69−Lys 6) CO bonds become longer. Most of these hydrogen bonds are present near the ligand binding site, and the observed changes in hydrogen bond lengths could be associated with the conformational changes occurring upon ligand binding. One hydrogen bond, HN (Phe 4−Ser 65) CO, displayed signal overlap in free ubiquitin, while in the complex, it could not be detected. This could be due to an increase in the R_2 relaxation rate and its consequent effect on the magnetization transfer. Qualitatively, we observed that the HN (Ile 23−Arg 54) CO hydrogen also becomes longer, thus relaying the dynamic changes to helix I. Via combination of our $^{h3}J_{NC'}$ trans hydrogen bond coupling results with the X-ray data of ubiquitin complexes, it is conceivable that the entire backbone of ubiquitin is capable of undergoing minor adjustments in response to ligand interaction by virtue of its unique interstrand backbone hydrogen bond network, despite the rigidity enforced by the hydrophobic core. A good correlation is observed between the sites displaying millisecond motions and the sites experiencing changes in hydrogen bond length in our solution studies, implying that they are correlated (Figure 9C,D). These observations support the recent findings, one with ubiquitin and the other with protein G, that elucidate the importance of interstrand hydrogen bonds in mediating the transfer of structural and dynamic information across the backbone.[57,58]

Finally, our solution studies combined with the X-ray data offer a unique window for improving our understanding of the process of ligand recognition by ubiquitin. During hydrogen bond analysis, we came across several instances in which the ubiquitin molecules present in the complexes drastically vary within the same unit cell, offering a sneak peek into the high-energy conformations. For instance, in PDB entry 3C0R, the N (Phe 45−Lys 48) CO hydrogen bond for the two ubiquitin molecules, each complexed to the ovarian tumor domain present in a single unit cell, displayed lengths of 2.58 and 3.3 Å, differing by more than 0.7 Å (Figure 4N of the Supporting Information), suggesting that the latter is a high-energy conformation. Structural comparison suggests forward movement of the $\beta_3-\alpha_2$ loop in the direction of the ligand in the latter case. In PDB entry 1WR6, the N (Leu 50−Leu 43) CO hydrogen bond in one of the four molecules displays a length of 3.8 Å, while in the rest of the molecules, this bond length is 2.8−2.9 Å (Figure 4V of the Supporting Information). In the structure, the backbone of Leu 50 is slightly distant from the ligand compared to the other three molecules, suggesting that it is a low-energy conformer. In PDB entry 2FIF, of the three molecules present in the unit cell, one displays a slightly longer N (Lys 6−Leu 67) CO hydrogen bond (∼3.05 Å) while the other two have lengths of 2.87 and 2.86 Å (Figure 4D of the Supporting Information). The crystal structure suggests that the $\beta_1-\beta_2$ loop is a little behind the other two in the former case. In one of the six molecules present in PDB entry 2C7N, the N (Gln 31−Lys 27) CO hydrogen bond length is 3.29 Å as opposed to ∼2.9 Å in the rest of the molecules, very similar to the results of our solution studies (Figure 4J of the Supporting Information). Similarly, in PDB entry 2ZNV, a 1.6 Å resolution structure, the N (Arg 42−Val 70) CO hydrogen bond in one of the four structures (chain ID C) present in the unit cell has a length of 4.0 Å (Figures 4AF and 5 of the Supporting Information), as opposed to the other three (2.82, 2.86, and 3.01 Å). Likewise, in PDB entry 3A9J, a 1.18 Å resolution structure, the same hydrogen bond is 3.63 Å long in one molecule and 2.79 Å long in the other (Figure 4AF of the Supporting Information). So many instances of such a remarkable change in hydrogen bond length are highly unusual and report on the intrinsic dynamics trapped during crystallization. We speculate that these outliers are snapshots of ubiquitin experiencing slow motions upon ligand binding. An important question we are trying to understand is whether the observed slow dynamics is a consequence of the ligand association−dissociation process. A recent study of dihydrofolate reductase (DHFR) and its inhibitors has shown that the switching of conformations from high energy to low energy correlates exponentially with K_i and K_{off}, indicating that the slow motions serve as a mechanical initiator of ligand dissociation when the protein is fully saturated with the ligand.[59] Comparison of the exchange rates obtained from the ^{15}N relaxation dispersion experiments with the ubiquitin−UIM complex ($k_{ex} \sim 3505\ s^{-1}$) with the ubiquitin−UIM association−dissociation rate ($\sim 13.7 \times 10^5\ s^{-1}$) clearly indicates that the former is an altogether different process.

Then, what is the physicochemical nature of the millisecond motions induced upon UIM interaction? Our relaxation dispersion experiments clearly suggest that there is more than one excited state in the UIM-complexed ubiquitin, though we have been able to characterize only the one that influences a majority of the residues. On the basis of $^{15}N-^{13}C$-filtered, ^{15}N-edited NOE experiments and insights from previous studies,[8,36,54] the UIM peptide is held firmly by two side chain to backbone hydrogen bonds, i.e., (a) Ser 183 side chain−Ala 46/Gly 47 HN bond of ubiquitin and (b) Glu 174 carboxyl of the UIM−Leu 73 HN bond of ubiquitin. The slow motions that we characterized display a maximum at the Ala 46 amide (maximal line broadening) that allows us to speculate that the side chain (UIM) to backbone (ubiquitin) hydrogen bond triggers these motions. Comparison of the distances between the Ser 183 side chain O atom of the UIM and the amide nitrogens of Ala 46 and Gly 47 yields values of ∼2.90 and 3.33 Å, respectively, for chain A and 3.69 and 2.82 Å, respectively, for chain B in PDB entry 2D3G, suggesting that both amides are equidistant from the Ser 183 O atom. Interestingly, both the amides face the ligand in a very similar fashion, suggesting that they are equally accessible to the ligand. Conceivably, the Ser 183 side chain of the UIM forms a bifurcated/fluctuating hydrogen bond with these two amide nitrogens simultaneously, giving rise to the unique dynamics that we observe in our relaxation experiments. This argument is further substantiated by (a) the observation of very similar downfield chemical shift changes in the backbone amides of Ala 46 and Gly 47 of 0.2 and 0.16 ppm, respectively, upon UIM interaction and (b) NOEs of equal intensity from both the amides (Ala 46 and Gly 47) to the H_β atom of Ser183 of the UIM in our filtered experiments (Figure 7A,B). We presume that the fluctuating nature of the hydrogen bond possibly gives rise to the motions. As the hydrogen bond draws the two binding partners close, it causes strain at three distinct sites in ubiquitin that interact with the ligand, i.e., Gly 47, Leu 8, and Leu 73. We speculate that these three sites act as epicenters of dynamic perturbations, relaying motions to the adjoining residues via the hydrogen bond network.

Altogether, the process of ligand recognition by ubiquitin can be summarized as noticeable changes in side chain conformation, backbone conformation, dynamics, and hydrogen bond lengths at sites that physically interact with the ligand, which in turn is caused by minor adjustments in hydrogen bond lengths all along the protein length. This is one of the first few studies that provide a quantitative measure of the backbone conformational changes in ubiquitin upon ligand binding. We speculate that (A) the exposed hydrophobic patch, (B) the unusual flexibility of the loops and the C-terminus, (C) the flexibility of the backbone hydrogen bonds, and (D) the highly flexible side chains make ubiquitin an excellent protein−protein interaction partner. Presumably, the initial phase of recognition is mediated by long-range electrostatic interactions and hydrophobic interactions, followed by conformational adjustments of the $\beta_1-\beta_2$ loop, the $\beta_3-\alpha_2$ loop, and strand β_4 to accommodate the ligand, which was also the conclusion reached by a recent study.[60] Thus, by sampling multiple conformations at the three sites, ubiquitin fine-tunes its interactions with its binding partners.

■ ASSOCIATED CONTENT

Supporting Information

Supplemental Figures 1−5. This material is available free of charge via the Internet at http://pubs.acs.org.

■ AUTHOR INFORMATION

Corresponding Author

*E-mail: monicasundd@nii.res.in. Phone: 011-91-26703823. Fax: 011-92-26742125.

Funding

I thank the Department of Biotechnology, Government of India, for financial support in the form of a grant as well as infrastructure support for the NMR facility at the National Institute of Immunology, New Delhi.

Notes

The authors declare no competing financial interest.

■ ACKNOWLEDGMENTS

The author thanks Ms. Arshdeep Sidhu for protein expression.

■ ABBREVIATIONS

UIM, ubiquitin interacting motif; HSQC, heteronuclear single-quantum coherence.

■ REFERENCES

(1) Raasi, S., Varadan, R., Fushman, D., and Pickart, C. M. (2005) Diverse polyubiquitin interaction properties of ubiquitin-associated domains. *Nat. Struct. Mol. Biol. 12*, 708−714.

(2) Bienko, M., Green, C. M., Crosetto, N., Rudolf, F., Zapart, G., Coull, B., Kannouche, P., Wider, G., Peter, G. M., Lahmann, A. R., Hofmann, K., and Dikic, I. (2005) Ubiquitin-binding domains in Y-family polymerases regulate translesion synthesis. *Science 310*, 1821−1824.

(3) Chen, Z. J., and Sun, L. (2009) Nonproteolytic functions of ubiquitin in cell signaling. *Mol. Cell 33*, 275−286.

(4) Hicke, L., Schubert, H. L., and Hill, C. P. (2005) Ubiquitin-binding domains. *Nat. Rev. Mol. Cell Biol. 6*, 610−621.

(5) Reyes-Turcu, F. E., Horton, J. R., Mullally, J. E., Heroux, A., Cheng, X., and Wilkinson, K. D. (2006) The ubiquitin binding domain ZnF UBP recognizes the C-terminal diglycine motif of unanchored ubiquitin. *Cell 124*, 1197−1208.

(6) Penengo, L., Mapelli, M., Murachelli, A. G., Confalonieri, S., Magri, L., Musacchio, A., Fiore, P. P., Polo, S., and Schneider, T. R. (2006) Crystal structure of the ubiquitin binding domains of Rabex-5 reveals two modes of interaction with ubiquitin. *Cell 124*, 1183−1195.

(7) Lee, S., Tsai, Y. C., Mattera, R., Smith, W. J., Kostelansky, M. S., Weissman, A. M., Bonifacino, J. S., and Hurley, J. H. (2006) Structural basis for ubiquitin recognition and autoubiquitination by Rabex-5. *Nat. Struct. Mol. Biol. 13*, 264−271.

(8) Sgourakis, N. G., Patel, M. M., Garcia, A. E., Makhatadze, G. I., and McCallum, S. A. (2010) Conformational dynamics and structural plasticity play critical roles in the ubiquitin recognition of a UIM domain. *J. Mol. Biol. 396*, 1128−1144.

(9) Lange, O. F., Lakomek, N.-A., Fares, C., Schroder, G. F., Walter, K. F. A., Becker, S., Meiler, J., Grubmuller, H., Griesinger, C., and de Groot, B. L. (2008) Recognition dynamics up to microseconds revealed from an RDC-derived ubiquitin ensemble in solution. *Science 320*, 1471−1475.

(10) Percia, T., and Chothia, C. (2010) Ubiquitin: Molecular mechanisms for recognition of different structures. *Curr. Opin. Struct. Biol. 20*, 367−376.

(11) Raiborg, C., Malerod, L., Pedersen, N. M., and Stenmark, H. (2008) Differential functions of Hrs and ESCRT proteins in endocytic membrane trafficking. *Exp. Cell Res. 314*, 801−813.

(12) Keskin, O., Tuncbag, N., and Gursoy, A. (2008) Characterization and prediction of protein interfaces to infer protein-protein interaction networks. *Curr. Pharm. Biotechnol. 9*, 67−76.

(13) Raiborg, C., Bache, K. G., Gillooly, D. J., Madshus, I. H., Stang, E., and Stenmark, H. (2002) Hrs sorts ubiquitinated proteins into clathrin-coated microdomains of early endosomes. *Nat. Cell Biol. 4*, 394−398.

(14) Fisher, R. D., Wang, B., Alam, S. L., Higginson, D. S., Robinson, H., Sundquist, W. I., and Hill, C. P. (2003) Structure and ubiquitin binding of the ubiquitin-interacting motif. *J. Biol. Chem. 278*, 28976−28984.

(15) Pan, P. W., Dickson, R. J., Gordon, H. L., Rothstein, S. M., and Tanaka, S. (2005) Functionally relevant protein motions: Extracting basin-specific collective coordinates from molecular dynamics trajectories. *J. Chem. Phys. 122*, 34904−34914.

(16) Lakomek, N. A., Lange, O. F., Walter, K. F., Fares, C., Egger, D., Lunkenheimer, P., Meiler, J., Grubmuller, H., Becker, S., deGroot, B. L., and Griesinger, C. (2008) Residual dipolar couplings as a tool to study molecular recognition of ubiquitin. *Biochem. Soc. Trans. 36*, 1433−1437.

(17) Fares, C., Lakomek, N. A., Walter, K. F., Frank, B. T., Meiler, J., Becker, S., and Griesinger, C. (2009) Accessing ns-micros side chain dynamics in ubiquitin with methyl RDCs. *J. Biomol. NMR 45*, 23−44.

(18) Mangia, S., Traaseth, N. J., Veglia, G., Garwood, M., and Michaeli, S. (2010) Probing slow protein dynamics by adiabatic $R_{1\rho}$ and $R_{2\rho}$ NMR experiments. *J. Am. Chem. Soc. 132*, 9979−9981.

(19) Raiborg, C., and Stenmark, H. (2009) The ESCRT machinery in endosomal sorting of ubiquitylated membrane proteins. *Nature 458*, 445−452.

(20) Stringer, D. K., and Piper, R. C. (2011) A single ubiquitin is sufficient for cargo protein entry into MVBs in the absence of ESCRT ubiquitination. *J. Cell Biol. 192*, 229−242.

(21) Sundd, M., Iverson, N. M., Ibarra-Molero, B., Sanchez-Ruiz, J. M., and Robertson, A. D. (2002) Electrostatic interactions in ubiquitin. Stabilization of carboxylates by lysine amino groups. *Biochemistry 41*, 7586−7596.

(22) Delaglio, F., Grzesiek, S., Vuister, G. W., Zhu, G., Pfeifer, J., and Bax, A. (1995) NMRPipe: A multidimensional spectral processing system based on UNIX pipes. *J. Biomol. NMR 6*, 277−293.

(23) Goddard, T. D., and Kneller, D. G. (2010) *SPARKY 3*, University of California, San Francisco.

(24) Wishart, D. S., Bigam, C. G., Yao, J., Abildgaard, F., Dyson, H. J., Oldfield, E., Markley, J. L., and Sykes, B. D. (1995) ^{1}H, ^{13}C and ^{15}N chemical shift referencing in biomolecular NMR. *J. Biomol. NMR 6*, 135−140.

(25) Raiford, D. S., Fisk, C. L., and Becker, E. D. (1979) Calibration of methanol and ethylene glycol nuclear magnetic resonance thermometers. *Anal. Chem. 51*, 2050−2051.
(26) Li, Y., Zhang, Y., and Yan, H. (1996) Kinetic and thermodynamic characterizations of yeast guanylate kinase. *J. Biol. Chem. 271*, 28038−28044.
(27) Farrow, N. A., Muhandiram, R., Singer, A. U., Pascal, S. M., Kay, C. M., Gish, G., Shoelson, S. E., Pawson, T., Forman-Kay, J. D., and Kay, L. E. (1994) Backbone dynamics of a free and phosphopeptide-complexed Src homology 2 domain studied by ^{15}N NMR relaxation. *Biochemistry 33*, 5984−6003.
(28) Tollinger, M., Skrynnikov, N. R., Mulder, F. A., Forman-Kay, J. D., and Kay, L. E. (2001) Slow dynamics in folded and unfolded states of an SH3 domain. *J. Am. Chem. Soc. 123*, 11341−11352.
(29) Cole, R., and Loria, P. J. (2003) FAST-Modelfree: A program for rapid automated analysis of solution NMR spin-relaxation data. *J. Biomol. NMR 26*, 203−213.
(30) Bieri, M., and Gooley, P. (2011) Automated NMR relaxation dispersion data analysis using NESS. *BMC Bioinf. 12*, 421.
(31) Carver, J. P., and Richards, R. E. (1972) General 2-site solution for chemical exchange produced dependence of T2 upon Carr-Purcell pulse separation. *J. Magn. Reson. 6*, 89.
(32) Cordier, F., and Grzesiek, S. (1999) Direct observation of hydrogen bonds in proteins by interresidue $^{h3}J_{NC'}$ scalar couplings. *J. Am. Chem. Soc. 121*, 1601−1602.
(33) Alexandrescu, A. T., Snyder, D. R., and Abildgaard, F. (2001) NMR of hydrogen bonding in cold-shock protein A and an alaysis of the influence of crystallographic resolution on ion pairs of hydrogen bond lengths. *Protein Sci. 10*, 1856−1868.
(34) Cornilescu, G., Ramirez, B. E., Frank, M. K., Clore, G. M., Gronenborn, A. M., and Bax, A. (1999) Correlation between $^{3h}J_{NC'}$ amd hydrogen bond length in proteins. *J. Am. Chem. Soc. 121*, 6275−6279.
(35) Cordier, F., Wang, C., Grzesiek, S., and Nicholson, L. K. (2000) Ligand-induced strain in hydrogen bonds of the c-Src SH3 domain detected by NMR. *J. Mol. Biol. 304*, 497−505.
(36) Hirano, S., Kawasaki, M., Ura, H., Kato, R., Raiborg, C., Stenmark, H., and Wakatsuki, S. (2006) Double-sided ubiquitin binding of Hrs-UIM in endosomal protein sorting. *Nat. Struct. Mol. Biol. 13*, 272−277.
(37) Lim, J., Son, W.-S., Park, J. K., Kim, E. E., Lee, B.-J., and Ahn, H.-C. (2011) Solution structure of UIM and interaction of tandem ubiqutin binding domains in STAM1 with ubiquitin. *Biochem. Biophys. Res. Commun. 405*, 24−30.
(38) Hong, Y.-H., Ahn, H.-C., Lim, J., Kim, H.-M., Ji, H.-Y., Lee, S., Kim, J.-H., Park, E. Y., Song, H. K., and Lee, B.-J. (2009) Identification of a novel ubiquitin binding site of STAM1 VHS domain by NMR spectroscopy. *FEBS Lett. 583*, 287−292.
(39) Tomlinson, J. H., Green, V. L., Baker, P. J., and Williamson, M. P. (2010) Structural origins of pH-dependent chemical shifts in the B1 domain of protein G. *Proteins 78*, 3000−3016.
(40) Wishart, D. S., Sykes, B. D., and Richards, F. M. (1991) Relationship between nuclear magnetic resonance chemical shift and protein secondary structure. *J. Mol. Biol. 222*, 311−333.
(41) Iwadate, M., Asakura, T., and Williamson, M. P. (1999) Cα and Cβ carbon-13 chemical shifts in proteins from an empirical database. *J. Biomol. NMR 13*, 199−211.
(42) Xu, X.-P., and Case, D. A. (2002) Probing multiple effects on ^{15}N, ^{13}Cα, ^{13}Cβ and ^{13}C′ chemical shifts in peptides using density functional theory. *Biopolymers 65*, 408−423.
(43) Tousignant, A., and Pelletier, J. N. (2004) Protein motions promote catalysis. *Chem. Biol. 11*, 1037−1042.
(44) Masterson, L. R., Shi, L., Metcalfe, E., Gao, J., Taylor, S. S., and Veglia, G. (2011) Dynamically committed, uncommitted, and quenched states encoded in protein kinase A revealed by NMR spectroscopy. *Proc. Natl. Acad. Sci. U.S.A. 108*, 6969−6974.
(45) Liu, J., Zhang, J., Yang, Y., Huang, H., Shen, W., Hu, Q., Wang, X., Wu, J., and Shi, Y. (2008) Conformational change upon ligand binding and dynamics of the PDZ domain from leukemia-associated Rho guanine nucleotide exchange factor. *Protein Sci. 17*, 1003−1014.
(46) Sidhu, A., Surolia, A., Robertson, A. D., and Sundd, M. (2011) A hydrogen bond regulates slow motions in ubiquitin by modulating a β-turn flip. *J. Mol. Biol. 411*, 1037−1048.
(47) Massi, F., Johnson, E., Wang, C., Rance, M., and Palmer, A. G. (2004) NMR R1p rotating-frame relaxation with weak radio frequency fields. *J. Am. Chem. Soc. 126*, 2247−2256.
(48) Hansen, D. F., Feng, H., Zhou, Z., Bai, Y., and Kay, L. E. (2009) Selective characterization of microsecond motions in proteins by NMR relaxation. *J. Am. Chem. Soc. 131*, 16257−16265.
(49) Lepre, C. A., Moore, J. M., and Peng, J. W. (2004) Theory and applications of NMR-based screening in pharmaceutical research. *Chem. Rev. 104*, 3641−3675.
(50) Clore, G. M., Szabo, A., Bax, A., Kay, L. E., Driscoll, P. C., and Gronenborn, A. M. (1990) Deviations from the simple two-parameter model-free approach to the interpretation of nitrogen-I5 nuclear magnetic resonance of proteins. *J. Am. Chem. Soc. 112*, 4989−4991.
(51) Huang, K. Y., Amodeo, G. A., Tong, L., and McDermott, A. (2011) The structure of human ubiquitin in 2-methyl-2,4-pentanediol: A new conformational switch. *Protein Sci. 20*, 630−639.
(52) Shen, Y., and Bax, A. (2010) SPARTA+: A modest improvement in empirical NMR chemical shift prediction by means of artificial neural network. *J. Biomol. NMR 48*, 13−22.
(53) Pettersen, E. F., Goddard, T. D., Huang, C. C., Couch, G. S., Greenblatt, D. M., Meng, E. C., and Ferrin, T. E. (2004) UCSF Chimera: A visualization system for exploratory research and analysis. *J. Comput. Chem. 25*, 1605−1612.
(54) Swanson, K. A., Kang, R. S., Stamenova, S. D., Hicke, L., and Radhakrishnan, I. (2003) Solution structure of Vps27 UIM-ubiquitin complex important for endosomal sorting and receptor down-regulation. *EMBO J. 22*, 4597−4606.
(55) Ohno, A., Jee, J., Fujiwara, K., Tenno, T., Goda, N., Tochio, H., Kobayashi, H., Hiroaki, H., and Shirakawa, M. (2005) Structure of the UBA domain of Dsk2p in complex with ubiqutin molecular determinants for ubiqutin recognition. *Structure 13*, 521−532.
(56) Sato, Y., Yoshikawa, A., Mimura, H., Yamashita, M., Yamagata, A., and Fukai., S. (2009) Structural basis for specific recognition of Lys 63-linked polyubiquitin chains by tandem UIMs of RAP80. *EMBO J. 28*, 2461−2468.
(57) Fenwick, R. B., Esteban-Martin, S., Richter, B., Lee, D., Walter, K. F. A., Milovanovic, D., Becker, S., Lakomek, N. A., Griesinger, C., and Salvatella, X. (2011) Weak long-range correlated motions in a surface patch of ubiquitin involved in molecular recognition. *J. Am. Chem. Soc. 133*, 10336−10339.
(58) Bouvignies, G., Bernado, P., Meier, S., Cho, K., Grzesiek, S., Bruschweiler, R., and Blackledge, M. (2005) Identification of slow correlated motions in proteins using residual dipolar and hydrogen-bond scalar couplings. *Proc. Natl. Acad. Sci. U.S.A. 102*, 13885−13890.
(59) Carroll, M. J., Maulding, R. V., Gromova, A. V., Singleton, S. F., Collins, E. J., and Lee, A. L. (2012) Evidence for dynamics in proteins as a mechanism for ligand dissociation. *Nat. Chem. Biol. 8*, 246−252.
(60) Holstein, M. A., Chung, W. K., Parimal, S., Freed, A. S., Barquera, B., McCallum, S. A., and Cramer, S. M. (2012) Probing multimodal ligand binding regions on ubiquitin using nuclear magnetic resonance, chromatography, and molecular dynamics simulations. *J. Chromatogr., A 1229*, 113−120.
(61) Koradi, R., Billeter, M., and Wuthrich, K. (1996) MOLMOL: A program for display and analysis of macromolecular structures. *J. Mol. Graphics 14*, 51−55.